2011

Stacked-and-drawn metamaterials with magnetic resonances in the terahertz range

Alessandro Tuniz
University of Sydney

Richard Lwin
University of Sydney

Alex Argyros
University of Sydney

Simon Fleming
University of Sydney

Elise Pogson
University of Wollongong, elisep@uow.edu.au

See next page for additional authors

Stacked-and-drawn metamaterials with magnetic resonances in the terahertz range

Alessandro Tuniz,[1,*] Richard Lwin,[1] Alexander Argyros,[1] Simon C. Fleming,[1] Elise M. Pogson,[2] Evan Constable,[2] Roger A. Lewis,[2] and Boris T. Kuhlmey[1]

[1]*Institute of Photonics and Optical Science (IPOS) and School of Physics, University of Sydney, Camperdown, New South Wales 2006, Australia*

[2]*Institute for Superconducting and Electronic Materials, University of Wollongong, Wollongong, New South Wales 2522, Australia*

[*]*alessandro.tuniz@sydney.edu.au*

Abstract: We present a novel method for producing drawn metamaterials containing slotted metallic cylinder resonators, possessing strong magnetic resonances in the terahertz range. The resulting structures are either spooled to produce a 2-dimensional metamaterial monolayer, or stacked to produce three-dimensional multi-layered metamaterials. We experimentally investigate the effects of the resonator size and number of metamaterial layers on transmittance, observing magnetic resonances between 0.1 and 0.4 THz, in good agreement with simulations. Such fibers promise future applications in mass-produced stacked or woven metamaterials.

OCIS codes: (160.2290) Fiber materials; (160.3918) Metamaterials.

References and links

1. W. Cai and V. Shalaev, *Optical metamaterials: fundamentals and applications* (Springer Verlag, 2009).
2. Z. Liu, H. Lee, Y. Xiong, C. Sun, and X. Zhang, "Far-field optical hyperlens magnifying sub-diffraction-limited objects," Science **315**(5819), 1686 (2007).
3. P. A. Belov, G. K. Palikaras, Y. Zhao, A. Rahman, C. R. Simovski, Y. Hao, and C. Parini, "Experimental demonstration of multiwire endoscopes capable of manipulating near-fields with subwavelength resolution," Appl. Phys. Lett. **97**(19), 191905 (2010).
4. D. Schurig, J. J. Mock, B. J. Justice, S. A. Cummer, J. B. Pendry, A. F. Starr, and D. R. Smith, "Metamaterial electromagnetic cloak at microwave frequencies," Science **314**(5801), 977–980 (2006).
5. V. M. Shalaev, "Optical negative-index metamaterials," Nat. Photonics **1**(1), 41–48 (2007).
6. N. I. Landy, S. Sajuyigbe, J. J. Mock, D. R. Smith, and W. J. Padilla, "Perfect metamaterial absorber," Phys. Rev. Lett. **100**(20), 207402 (2008).
7. A. Boltasseva and V. M. Shalaev, "Fabrication of optical negative-index metamaterials: Recent advances and outlook," Metamaterials (Amst.) **2**(1), 1–17 (2008).
8. M. Walther, A. Ortner, H. Meier, U. Loffelmann, P. J. Smith, and J. G. Korvink, "Terahertz metamaterials fabricated by inkjet printing," Appl. Phys. Lett. **95**(25), 251107 (2009).
9. K. Takano, T. Kawabata, C. F. Hsieh, K. Akiyama, F. Miyamaru, Y. Abe, Y. Tokuda, R. P. Pan, C. L. Pan, and M. Hangyo, "Fabrication of terahertz planar metamaterials using a super-fine ink-jet printer," Appl. Phys. Express **3**, 016701 (2010).
10. H. Kim, J. S. Melinger, A. Khachatrian, N. A. Charipar, R. C. Y. Auyeung, and A. Piqué, "Fabrication of terahertz metamaterials by laser printing," Opt. Lett. **35**(23), 4039–4041 (2010).
11. H. Tao, A. C. Strikwerda, K. Fan, C. M. Bingham, W. J. Padilla, X. Zhang, and R. D. Averitt, "Terahertz metamaterials on free-standing highly-flexible polyimide substrates," J. Phys. D Appl. Phys. **41**(23), 232004 (2008).
12. X. G. Peralta, M. C. Wanke, C. L. Arrington, J. D. Williams, I. Brener, A. Strikwerda, R. D. Averitt, W. J. Padilla, E. Smirnova, A. J. Taylor, and J. F. O'Hara, "Large-area metamaterials on thin membranes for multilayer and curved applications at terahertz and higher frequencies," Appl. Phys. Lett. **94**(16), 161113 (2009).
13. A. Tuniz, B. T. Kuhlmey, R. Lwin, A. Wang, J. Anthony, R. Leonhardt, and S. C. Fleming, "Drawn metamaterials with plasmonic response at terahertz frequencies," Appl. Phys. Lett. **96**(19), 191101 (2010).
14. X. Zhang, Z. Ma, Z. Y. Yuan, and M. Su, "Mass-productions of vertically aligned extremely long metallic micro/nanowires using fiber drawing nanomanufacturing," Adv. Mater. (Deerfield Beach Fla.) **20**(7), 1310–1314 (2008).
15. A. F. Abouraddy, M. Bayindir, G. Benoit, S. D. Hart, K. Kuriki, N. Orf, O. Shapira, F. Sorin, B. Temelkuran, and Y. Fink, "Towards multimaterial multifunctional fibres that see, hear, sense and communicate," Nat. Mater. **6**(5), 336–347 (2007).

#150223 - $15.00 USD Received 30 Jun 2011; revised 22 Jul 2011; accepted 22 Jul 2011; published 11 Aug 2011

16. E. Badinter, A. Ioisher, E. Monaico, V. Postolache, and I. M. Tiginyanu, "Exceptional Integration of Metal or Semimetal Nanowires in Human-Hair-Like Glass Fiber," Mater. Lett. **64**(17), 1902–1904 (2010).
17. C. G. Poulton, M. A. Schmidt, G. J. Pearce, G. Kakarantzas, and P. S. J. Russell, "Numerical study of guided modes in arrays of metallic nanowires," Opt. Lett. **32**(12), 1647–1649 (2007).
18. J. Hou, D. Bird, A. George, S. Maier, B. T. Kuhlmey, and J. C. Knight, "Metallic mode confinement in microstructured fibres," Opt. Express **16**(9), 5983–5990 (2008).
19. M. A. Schmidt, L. N. P. Sempere, H. K. Tyagi, C. G. Poulton, and P. S. J. Russell, "Waveguiding and plasmon resonances in two-dimensional photonic lattices of gold and silver nanowires," Phys. Rev. B **77**(3), 033417 (2008).
20. H. K. Tyagi, H. W. Lee, P. Uebel, M. A. Schmidt, N. Joly, M. Scharrer, and P. S. J. Russell, "Plasmon resonances on gold nanowires directly drawn in a step-index fiber," Opt. Lett. **35**(15), 2573–2575 (2010).
21. A. Mazhorova, J. F. Gu, A. Dupuis, M. Peccianti, O. Tsuneyuki, R. Morandotti, H. Minamide, M. Tang, Y. Wang, H. Ito, and M. Skorobogatiy, "Composite THz materials using aligned metallic and semiconductor microwires, experiments and interpretation," Opt. Express **18**(24), 24632–24647 (2010).
22. A. Tuniz, B. T. Kuhlmey, P. Y. Chen, and S. C. Fleming, "Weaving the invisible thread: design of an optically invisible metamaterial fibre," Opt. Express **18**(17), 18095–18105 (2010).
23. A. Wang, A. Tuniz, P. G. Hunt, E. M. Pogson, R. A. Lewis, A. Bendavid, S. C. Fleming, B. T. Kuhlmey, and M. C. J. Large, "Fiber metamaterials with negative magnetic permeability in the terahertz," Opt. Mater. Express **1**(1), 115–120 (2011).
24. J. B. Pendry, A. J. Holden, D. J. Robbins, and W. J. Stewart, "Magnetism from conductors and enhanced nonlinear phenomena," IEEE Trans. Microw. Theory Tech. **47**(11), 2075–2084 (1999).
25. M. C. K. Wiltshire, J. B. Pendry, W. Williams, and J. V. Hajnal, "An effective medium description of'Swiss Rolls', a magnetic metamaterial," J. Phys-Condens. Mat. **19**, 456216 (2007).
26. H. J. Schneider and P. Dullenkopf, "Slotted tube resonator: A new NMR probe head at high observing frequencies," Rev. Sci. Instrum. **48**(1), 68–73 (1977).
27. J. Du, S. Liu, Z. Lin, and S. T. Chui, "Magnetic resonance of slotted circular cylinder resonators," J. Appl. Phys. **104**(1), 014907 (2008).
28. C. E. Kriegler, M. S. Rill, M. Thiel, E. Müller, S. Essig, A. Frölich, G. von Freymann, S. Linden, D. Gerthsen, H. Hahn, K. Busch, and M. Wegener, "Transition between corrugated metal films and split-ring-resonator arrays," Appl. Phys. B **96**(4), 749–755 (2009).
29. M. S. Rill, C. E. Kriegler, M. Thiel, G. von Freymann, S. Linden, and M. Wegener, "Negative-index bianisotropic photonic metamaterial fabricated by direct laser writing and silver shadow evaporation," Opt. Lett. **34**(1), 19–21 (2009).
30. A. Argyros, "Microstructured polymer optical fibers," J. Lightwave Technol. **27**(11), 1571–1579 (2009).
31. M. A. van Eijkelenborg, A. Argyros, and S. G. Leon-Saval, "Polycarbonate hollow-core microstructured optical fiber," Opt. Lett. **33**(21), 2446–2448 (2008).
32. J. Anthony, R. Leonhardt, A. Argyros, and M. C. J. Large, "Characterization of a microstructured Zeonex terahertz fiber," J. Opt. Soc. Am. B **28**(5), 1013–1018 (2011).
33. http://www.zeonex.com.
34. K. Fan, A. C. Strikwerda, H. Tao, X. Zhang, and R. D. Averitt, "Stand-up magnetic metamaterials at terahertz frequencies," Opt. Express **19**(13), 12619–12627 (2011).
35. R. Y. Koyama, N. V. Smith, and W. E. Spicer, "Optical properties of indium," Phys. Rev. B **8**(6), 2426–2432 (1973).
36. Y. S. Jin, G. J. Kim, and S. G. Jeon, "Terahertz dielectric properties of polymers," J. Korean Phys. Soc. **49**, 513–517 (2006).
37. D. Grischkowsky, S. Keiding, M. Exter, and C. Fattinger, "Far-infrared time-domain spectroscopy with terahertz beams of dielectrics and semiconductors," J. Opt. Soc. Am. B **7**(10), 2006–2015 (1990).
38. E. M. Pogson, R. A. Lewis, M. Koeberle, and R. Jacoby, "Terahertz time-domain spectroscopy of nematic liquid crystals," in *Proc. SPIE*(2010), p. 77281Y.
39. R. W. Wood, "Anomalous Diffraction Gratings," Phys. Rev. **48**(12), 928–936 (1935).
40. A. E. Miroshnichenko, S. Flach, and Y. S. Kivshar, "Fano resonances in nanoscale structures," Rev. Mod. Phys. **82**(3), 2257–2298 (2010).
41. B. Luk'yanchuk, N. I. Zheludev, S. A. Maier, N. J. Halas, P. Nordlander, H. Giessen, and C. T. Chong, "The Fano resonance in plasmonic nanostructures and metamaterials," Nat. Mater. **9**(9), 707–715 (2010).
42. F. J. Rodríguez-Fortuño, B. Tomás-Navarro, C. García-Meca, R. Ortuño, J. Martí, and A. Martínez, "Zero-bandwidth mode in a split-ring-resonator-loaded one-dimensional photonic crystal," Phys. Rev. B **81**(23), 233101 (2010).
43. A. Ishikawa, S. Zhang, D. A. Genov, G. Bartal, and X. Zhang, "Deep subwavelength terahertz waveguides using gap magnetic plasmon," Phys. Rev. Lett. **102**(4), 043904 (2009).
44. M. Yan and N. A. Mortensen, "Hollow-core infrared fiber incorporating metal-wire metamaterial," Opt. Express **17**(17), 14851–14864 (2009).

1. Introduction

Metamaterials are man-made materials engineered to respond to electromagnetic fields in ways not observed in naturally occurring materials, and are produced via an arrangement of sub-wavelength yet macroscopic metallo-dielectric "atoms" [1]. A number of intriguing

#150223 - $15.00 USD Received 30 Jun 2011; revised 22 Jul 2011; accepted 22 Jul 2011; published 11 Aug 2011

metamaterial devices have so far been demonstrated, including sub-diffraction-limited lenses [2,3], electromagnetic cloaks [4] negative refractive index materials [5], and perfectly absorbing materials [6]. Generally, metamaterial fabrication from the terahertz (THz) into the visible however relies on techniques that limit total sample sizes to be no larger than a few cm^2, i.e. electron-beam lithography, nano-imprint lithography, focused-ion beam milling, and direct laser writing [7]. Low-cost mass-production of metamaterials is an important issue that has been addressed in recent years, for example using inkjet [8, 9] and laser [10] printing. Additionally, large-area flexible magnetic metamaterials have also been produced [11,12], which allow for easy handling and can adapt to three-dimensional surfaces.

Recently, fiber drawing has emerged as a novel way of inexpensively producing large amounts of metamaterials [13], potentially kilometers in length. With this technique, a macroscopic dielectric preform containing metals or semiconductors is heated and stretched to fiber, preserving the transverse structure, and reducing the scale while increasing the length. Clearly, this technique is well-suited for the mass production of longitudinally-invariant geometries [14], with a number of integrated fiber devices being envisioned [15]. Drawing has been used to produce fibers containing metallic micro- and nano-structured wires with diameters as small as 50 nm [16], with demonstrations of metallic mode confinement [17,18], plasmonic resonances [19, 20] and metamaterial high-pass filtering [13, 21] where the effective electric permittivity ε of the fiber can be tailored from THz to visible frequencies [22]. Fibers with retrieved negative effective permeability μ in the THz have also been produced, via a two-step procedure in which metal is sputtered onto a dielectric fiber of appropriate external shape [23]. It is worth noting that using this one technique, metamaterials over many frequency ranges can be realized.

Magnetically responsive metamaterials in the THz are more commonly produced by arranging sub-wavelength metallic split ring resonators (SRRs), i.e. planar open conductive split loops with a capacitance C and inductance L, that oppose incident magnetic fields near the LC resonant frequency. Here we fabricate slotted cylinder resonators in fiber form, which are longitudinally invariant split-ring resonators. They have a similar geometry to the "swiss-roll" metamaterials [24], which are formed by rolling alternating metal-dielectric films, and yield large effective negative magnetic permeability [25]. More than thirty years ago slotted cylinders found applications as nuclear magnetic resonance probes [26], but in recent years they have attracted attention as components of metamaterials exhibiting a negative magnetic response [27]. Slotted resonators have recently been produced for operation in the near- and mid-infrared via a combination of polymer direct-laser writing and chemical vapor deposition [28], with similar structures being arranged to produce negative-index metamaterials [29].

Here we present a procedure for producing hundreds of meters of metamaterial fibers with a magnetic response in the THz range, based on fabrication techniques developed for microstructured polymer optical fibers [30]. Two fabrication methods are outlined, which allow scalable metamaterial resonators; the first (direct-draw method) involves preparing a macroscopic polymer preform containing a slotted indium cylinder, heating it and drawing it directly to a fiber containing a single sub-wavelength magnetic resonator, and the second (stack-and-draw method) extends this procedure by arranging many such fibers in a rectangular preform, and subsequently re-drawing to a slab containing smaller resonators. Finally, we experimentally characterize the transmittance of single and multiple layers of such drawn structures in the terahertz frequency range, finding good agreement with numerical simulations, and evidence of Fano-like interplay between Bragg and magnetic resonances.

#150223 - $15.00 USD Received 30 Jun 2011; revised 22 Jul 2011; accepted 22 Jul 2011; published 11 Aug 2011

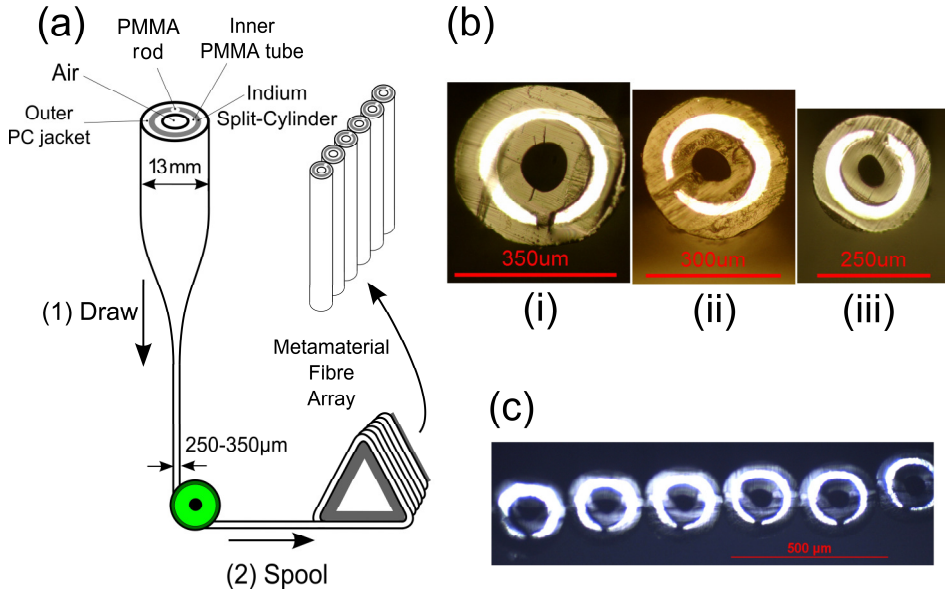

Fig. 1. (a) Schematic of the direct-draw fabrication procedure. A cm-sized preform consisting of an outer PC jacket, an indium slotted-cylinder and an inner PMMA tube is drawn into fiber and spooled into an array. The final array constitutes a metamaterial layer. (b) Optical microscope image of the cross section of (i) 350 μm, (ii) 300 μm and (iii) 250 μm fiber originating from the same preform. (c) Cross-sectional image of the spooled 250 μm fibers.

2. Fabrication and sample preparation

2.1 Direct-draw method

A schematic of the direct-draw fabrication procedure is summarized in Fig. 1(a). A 1 mm thick indium foil was rolled around a poly-methyl-methacrylate (PMMA) tube [outer diameter (OD) 7.5 mm, inner diameter (ID) 3.8 mm], together with a 1 mm PMMA rod, to produce a slotted cylinder. This structure was inserted into a polycarbonate (PC) jacket (13 mm OD, 10 mm ID). This structure was evacuated and drawn down to fiber under high tension (40-90 g) at temperatures of 200-220 °C. By varying the draw speed, we fabricated more than 100 m of fiber with diameters of 350 μm, 300 μm, and 250 μm. Figure 1(b) shows the cross-sectional optical microscope images of such fibers [(i), (ii) and (iii) respectively]. The metal is not continuous in the early stages of the draw, when the preform first heats and drops to fiber, but as the drawing conditions stabilize (i.e. temperature, draw/feed speed, and fiber tension) the metal is continuous throughout the entire drawing process. The resonator sizes are such that this is evident from visual inspection.

PMMA and PC were chosen because they are drawable dielectrics with appropriate optical properties. Indium was chosen because it possesses a melting temperature of 156.6 °C, so that the resonator-shaped metal wires remain liquid during the draw. The use of two different polymers was motivated by the uneven temperature profile within the fiber during the drawing process: the largely radiative heat transfer from the furnace is shielded by the indium sheet so that the core of the fiber does not reach temperatures as high as the jacket. If a single polymer was used, the core would be much stiffer than the surrounding material, making an even draw difficult. As PMMA has a lower glass transition temperature (T_g = 115 °C [30]) than PC (T_g = 150 °C [31]), our geometry maintains similar viscosities on either side of the indium sheet, in spite of the temperature contrast. The hole in the PMMA core further improves the heat and viscosity distribution by diminishing the total thermal capacity at the center.

To characterize the resonator transmittance (see Section 3) the fibers were spooled onto a triangular frame, each side of which produced a single flat array [Fig. 1(a)]. Figure 1(c) shows

#150223 - $15.00 USD Received 30 Jun 2011; revised 22 Jul 2011; accepted 22 Jul 2011; published 11 Aug 2011

a microscope image of the cross section of the 250 μm fiber array, indicating that the resonator shape stays constant throughout the draw process, and that the orientation of the resonators is maintained during the spooling process. This was indeed the case for all fiber arrays. Note that when the draw parameters are constant the fluctuations in fiber resonator cross-sections are barely noticeable, as is evident from Fig. 1(c). However, changing the drawing conditions (e.g. changing the draw speed to obtain different-sized resonators) affects the shape of the resonator and the gap size, as can be seen in the cross sections of Fig. 1(b)(i)-(iii).

2.2 Stack-and-draw method

To produce arrays of smaller resonators, the stack-and-draw method was used, summarized in Fig. 2(a). We prepared 20 m of 700 μm diameter fiber containing a metal slotted-cylinder resonator, following the procedure described in Section 2.1. The fiber was then cut into 30 cm pieces. Separately, we prepared a rectangular 2 × 6 cm^2 Zeonex [32, 33] polymer preform, in which we drilled a row of six 5 mm holes. This preform was then drawn down to a rectangular 12 × 3 mm^2 fiber under high tension. The fiber maintained its rectangular shape during the draw, however due to the proximity of the holes to the edge of the preform, the six holes deformed slightly, becoming elliptical in shape with a minor axis of ~700 μm.

Each 700 μm fiber containing a slotted resonator could thus be tightly fitted into each hole of the rectangular preform. The orientation of the resonators was adjusted by observing the location of the slot with the naked eye. This structure was drawn down to fiber under high tension (200-400 g) at temperatures of 170-190 °C. By varying the draw speed, we fabricated more than 10 m of rectangular fiber with widths between 1.5 mm and 1.9 mm. Figure 2(b) shows cross-sectional optical microscope images of such rectangular fibers of 1.9 mm, 1.7 mm and 1.5 mm widths [samples (i), (ii) and (iii) respectively]. The resonators contained therein scaled appropriately, with sizes of 130 μm, 115 μm, and 100 μm, respectively.

Owing to the fact that the circular resonator fibers were tightly fitted in elliptical holes before drawing, air gaps between the fiber resonators and the Zeonex are present, and can be seen as black crescents in Fig. 2(b). This could be avoided either by applying vacuum (which might deform the resonators in the drawing process), or by ensuring that the holes containing

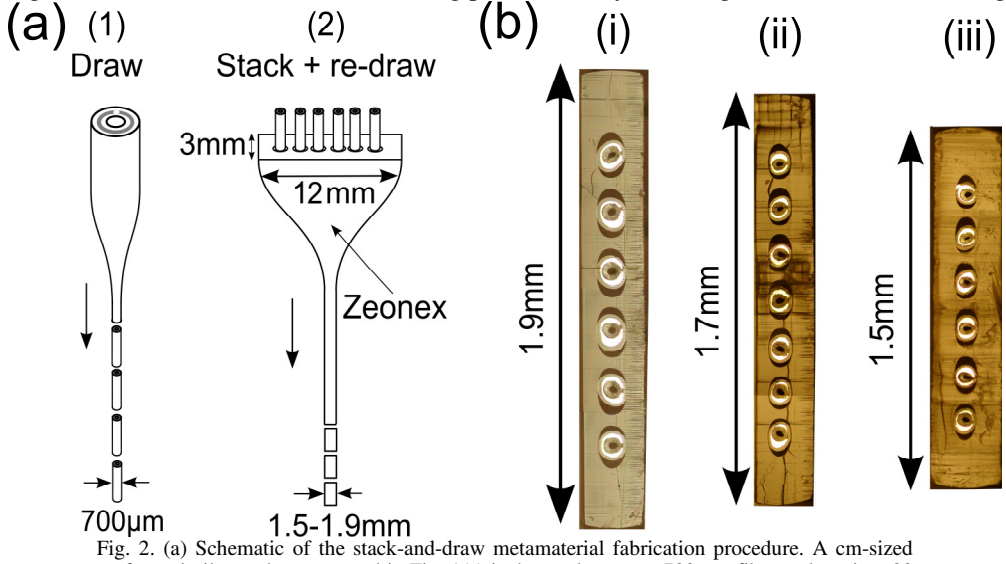

Fig. 2. (a) Schematic of the stack-and-draw metamaterial fabrication procedure. A cm-sized preform similar to that presented in Fig. 1(a) is drawn down to a 700 μm fiber and cut into 30 cm pieces. Each piece is inserted into the six holes of a 12 × 3 mm^2 rectangular Zeonex preform. This entire structure is re-drawn down to rectangular fibers of 1.5-1.9 mm. (b) Optical microscope image of the cross section of (i) 1.9 mm, (ii) 1.7 mm and (iii) 1.5 mm wide rectangular fiber, containing six slotted resonators. Note that fibers (i) and (ii) have been polished on the sides.

#150223 - $15.00 USD Received 30 Jun 2011; revised 22 Jul 2011; accepted 22 Jul 2011; published 11 Aug 2011

the resonator fibers are circular to begin with (for example by using a geometry with a smaller air filling fraction).

We cut 1 cm pieces of samples (i)-(iii), each of which consists of a robust metamaterial "chip"; additionally, we stacked 2, 3 and 6 layers of the 1.9 mm wide chip to make "bulk" metamaterial samples. Note that here we have used a rectangular slab geometry because it is best suited for characterizing the transmittance of the resonators contained therein. This procedure simplifies the production of continuous drawn metamaterial films [21], and can also be used to produce more intricate arrangements of resonators.

In the drawn resonators presented here and for TM incidence, the magnetic field is parallel to the fiber and thus has a nonzero magnetic flux through the resonator loop; the electric field is used to generate currents which couple directly to the magnetic resonance, in a similar fashion to the recently reported "stand-up" SRRs [34] which were produced via a multilayer electroplating technique. Most commonly however, arrays of thin SRRs are printed on substrates such that that the resonator loops are in the same plane as the array; for normal incidence, the magnetic field is then parallel to the plane of the resonator loops, has zero magnetic flux and is unable to excite a magnetic response directly. In contrast, a drawn resonator geometry lends itself well to direct magnetic resonator excitation [23].

3. Characterization

3.1 Direct-drawn fibers: experiment and simulation

The transmittance of our direct-drawn samples described in Section 2.1 was measured using a two-color system as a THz source. This source is composed of two lasers of wavelengths 853 nm and 855 nm that are combined using a GaAs antenna, producing a difference frequency radiation. The frequency difference is scanned from tens of GHz to THz by varying the temperatures of one of the lasers. A Schottky diode detector measures the intensity as a function of frequency (0.002 THz steps). The transmittance is defined as the ratio of the intensity transmitted with and without the metamaterial array. The results are shown in Fig. 3(a) (top), under TM illumination, i.e. the incident magnetic field H is directed along the fiber

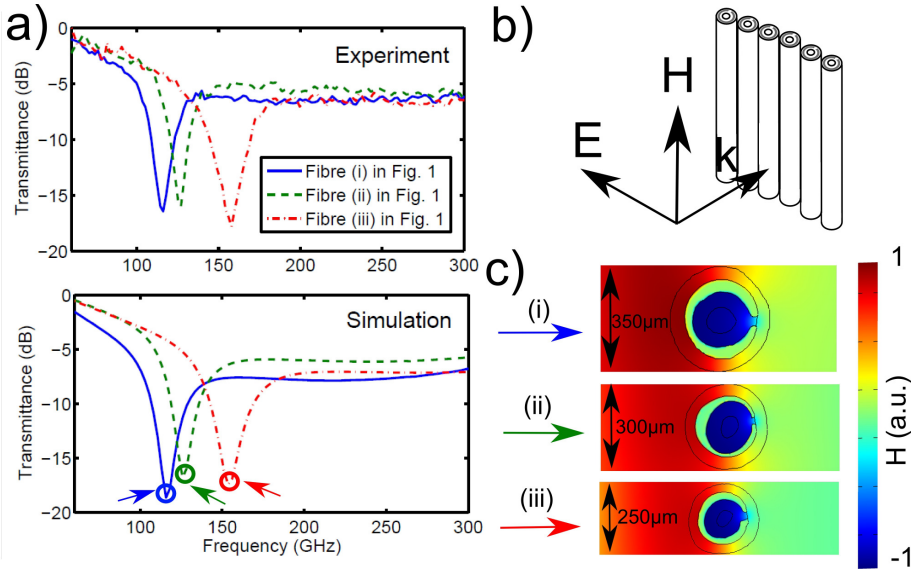

Fig. 3. (a) Experimentally measured (top) and simulated (bottom) transmittance for fibers (i), (ii), (iii) in Fig. 1. (b) The incident magnetic field is directed along the fibers. (c) Color plot of the simulated magnetic fields for each fiber at resonance indicated by the colored arrows and circles on (a).

#150223 - $15.00 USD Received 30 Jun 2011; revised 22 Jul 2011; accepted 22 Jul 2011; published 11 Aug 2011

- see [Fig. 3(b)]. Fibers (i)-(iii) in Fig. 1(b) exhibit transmission dips associated with a magnetic resonance at 116 GHz, 126 GHz and 158 GHz, respectively. Clearly, the resonant frequency increases as the resonators contained in the fibers scale down.

We modeled the transmittance of our resonator arrays using the finite element solver COMSOL, based on the photographed geometries. The appropriate orientation of the resonators within our fibers with respect to the incident field was taken into account in our simulations. The refractive indices for PMMA, PC and indium taken from Refs [35, 36] were used in this range. We obtained the scattering matrix parameters numerically, finding excellent agreement between experimental and simulated transmittance for all fiber sizes [Fig. 3(a), bottom]. A density plot of the magnetic field at resonance for each of the fibers is shown in Fig. 3(c); the magnetic field inside the resonator opposes the incident field in each case, indicating strong magnetic resonances.

3.2 Stack-and-drawn fibers: experiment and simulation

The transmittance of our stacked-and-drawn samples was measured between 0.2 and 1 THz via THz time domain spectroscopy [37, 38]. We used lenses to focus the THz field down to a spot size of approximately 1 mm; our mm-sized samples were placed at this focal point. The transmission of electric field pulses was measured in the time domain for the metamaterial arrays and for air. The power spectrum for each was then calculated through a magnitude squared Fourier transform. The transmittance was obtained by dividing the intensity recorded after transmission through the sample by the intensity without the sample. Figure 4(a) (top) shows the experimental results for TM illumination [see Fig. 4(b)]. Samples (i)-(iii) in Fig. 2(b) exhibit transmission dips associated with a magnetic resonance at 0.31 THz, 0.35 THz and 0.39 THz, respectively; once again, the resonant frequencies increase as the resonators scale down.

For the numerical characterization, we imported the optical microscope image of the 1.9 mm wide rectangular sample of Fig. 2(b)(i) into COMSOL, included the appropriate dispersive optical properties for all materials, and obtained the transmittance via the scattering matrix parameters for the central 1.6 mm region of the sample, corresponding to the focused beam. For numerical characterization of the smaller rectangular samples (1.7 mm and 1.5 mm wide) we modeled a scaled-down version of the 1.9 mm sample geometry. In all cases, we find good agreement with experiment for all resonator sizes [Fig. 4(a), bottom]. A density plot of the magnetic field at resonance for one of the resonators contained in the rectangular sample is shown in Fig. 4(c) – clearly the magnetic field inside the resonator opposes the incident field in each case, once again an indication of a strong magnetic resonance.

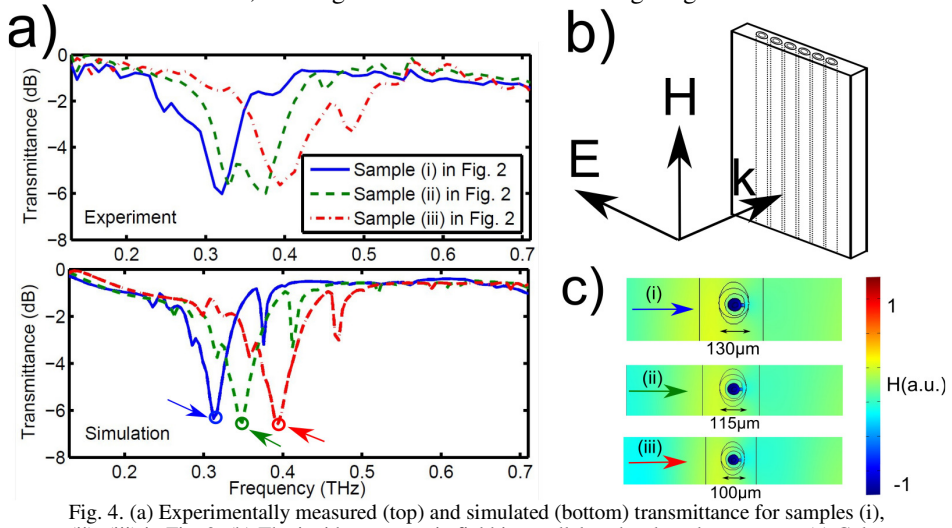

Fig. 4. (a) Experimentally measured (top) and simulated (bottom) transmittance for samples (i), (ii), (iii) in Fig. 2. (b) The incident magnetic field is parallel to the slotted resonators. (c) Color plot of the simulated magnetic fields at resonance for one resonator in the slab.

#150223 - $15.00 USD Received 30 Jun 2011; revised 22 Jul 2011; accepted 22 Jul 2011; published 11 Aug 2011

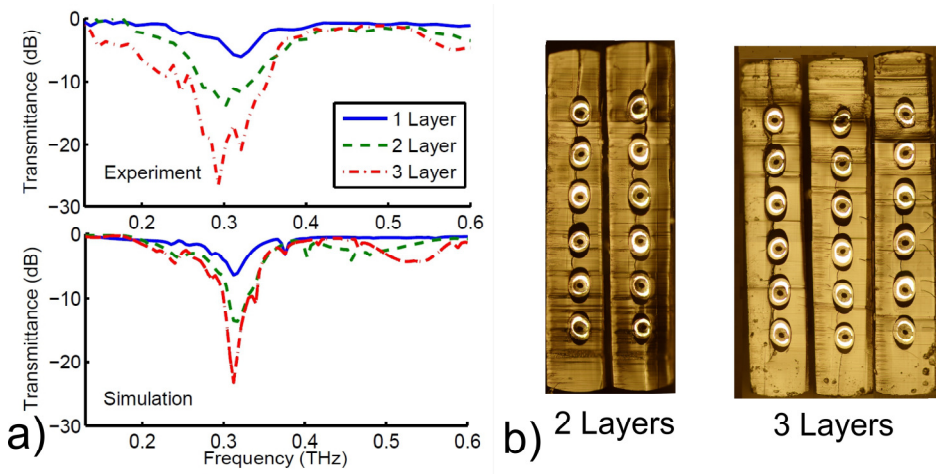

Fig. 5. (a) Experimentally measured (top) and simulated (bottom) transmittance for 1, 2, and 3 layers of sample (i) shown in Fig. 2. (b) Optical microscope images of the 2- and 3-layer fiber samples.

Figure 5(a) (top) shows the experimental transmittance for 1, 2 and 3 layers of the 1.9 mm sample (i) of Fig. 2(b). Such multi-layer arrays were manually stacked and glued together at one end, demonstrating the robustness and ease of handling of the rectangular fibers produced. Figure 5(b) shows cross-sectional optical microscope images of such multi-layer rectangular fiber arrays. As expected, the transmittance dip associated with the magnetic resonance increases with number of layers, in agreement with simulations, shown in Fig. 5(a) (bottom). In this case the structures were modeled by including one, two and three adjacent layers of the 1.9 mm metamaterial slab described in the previous paragraph; a detail of the single layer case is shown in Fig. 3(c)(top).

Note that for multiple sample layers, the separation between adjacent resonator arrays is given by the width of the rectangular fiber containing them, which in this case is ~400 μm. For normal incidence and assuming perfect scatterers, one expects N^{th} order resonant Bragg-reflection at a wavelength $\lambda_B = 2nd/N$, where n is the average refractive index of the background medium (Zeonex, n = 1.52 [32]), and d = 400 μm is the separation between resonators. First-order (N = 1) Bragg reflection thus occurs at a wavelength λ_B = 610 μm, corresponding to a Bragg reflection frequency f_B = 0.25 THz, which is close to the resonant frequency observed for the single-layer case, f_R = 0.31 THz. Therefore, even though the ratio between resonator diameter (D = 130μm) and resonant wavelength (λ_R = 970 μm) is small (D/λ_R = 0.13), for the multiple-layer case the magnetic resonance nearly overlaps the Bragg resonance. It thus becomes necessary to consider how each resonance might contribute to the overall transmittance spectrum in the multi-layer case.

For this purpose, we considered the 3-layer stack. We numerically investigated how the transmittance of our resonator arrays varies with different separation between resonator arrays, assuming a Zeonex background. We considered separations d = 200 μm, 300 μm, 400 μm, 500 μm, corresponding to first-order Bragg reflection frequencies f_B = 0.49 THz, 0.33 THz, 0.25 THz, and 0.2 THz, respectively. The results are shown in Fig. 6(a) (red dashed line).

For d = 200 μm, the Bragg resonance and the magnetic resonance clearly occur at distinct frequencies, 0.5 THz and 0.3 THz, respectively. The two resonances differ by more than 20 dB in depth, indicating that the magnetic resonance is significantly stronger than the Bragg resonance. For larger separations, the Bragg resonance frequency decreases and begins to overlap with the magnetic resonance. Note that while the magnetic resonance occurs at the

#150223 - $15.00 USD Received 30 Jun 2011; revised 22 Jul 2011; accepted 22 Jul 2011; published 11 Aug 2011

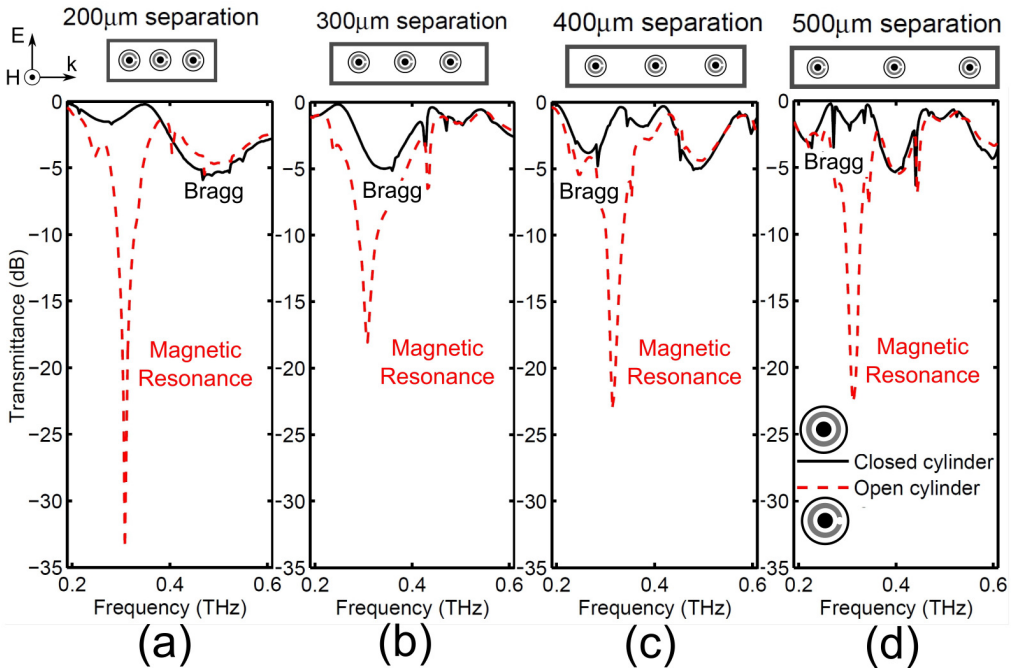

Fig. 6. Comparison of the numerically obtained transmittance for open cylinders and closed cylinders for the three-layer case with different separations between cylinders.

same frequency independently of d, its depth changes for different resonator separations. Interestingly, if we increase the resonator separation to d = 300 μm, i.e. near the Bragg resonance [Fig. 6(b)], the resonance broadens asymmetrically and transmittance increases by 15 dB. Further increasing the separation to d = 400 μm or d = 500 μm leads to a reduction in resonant transmittance by 5 dB. Thus, the overall resonance depth and breadth depend strongly on resonator separation.

To gain further insight, we numerically modeled the transmittance of the same geometries, but for *closed* cylinders, removing the capacitance and thus the LC (magnetic) resonance, so that dips in transmission are solely due to Bragg scattering. The results are shown in black lines in Fig. 6. For d = 200 μm [Fig. 6(a)], the Bragg resonance closely matches that of its open-cylinder counterpart, and the magnetic resonance is absent. For d = 300 μm [Fig. 6(b)], the Bragg resonance nearly overlaps the magnetic resonance, but for larger separations still [Fig. 6(c)-(d)] the Bragg resonance is again detuned from the magnetic resonance. Additionally, note that very fine, sharp transmission dips occasionally appear in the simulated spectra for both open and closed cylinders, e.g. at frequencies of 0.27 THz and 0.44 THz in Fig. 6(d); these features are due to coupling to vertically propagating modes of the metamaterial slab, similar to the coupling to surface modes and passing of gratings orders known as Wood anomalies [39].

The significant increase in transmittance for a separation d = 300 μm is thus likely due to a constructive interference occurring between the overlapping slotted cylinder resonance and Bragg resonance, which can change the balance between reflection and transmission via a Fano resonance behavior [40]. Fano resonances in metamaterials have recently attracted considerable attention [41]: note, for example, that a geometry similar to the one presented here is presented in Ref [42] for applications in electromagnetic-induced transparency, slow-light, and time-reversal. Such geometries could potentially be assembled for operation in the THz using components similar to the ones presented here. This will be a subject of future study.

Finally, we measured the transmittance of a sample containing six stacked 1.9 mm samples (i) of Fig. 2(b) under TM polarization. This sample is particularly interesting because

#150223 - $15.00 USD Received 30 Jun 2011; revised 22 Jul 2011; accepted 22 Jul 2011; published 11 Aug 2011

it is composed of a metamaterial "cube" of six layers of six resonators. The experimental results are shown in Fig. 7(a) (top). Figure 7(b) shows an optical microscope image of the cross-section of the six-layer metamaterial. Here we consider two directions of incidence, labeled as "direction 1" and "direction 2"; in practice, the sample was simply rotated with respect to the incident field. For both directions of incidence, a magnetic resonance is observed near 0.3 THz, as expected. Additionally, for the incident field propagating in "direction 2", a first-order Bragg resonance is observed at 0.4 THz, since in that orientation the layer-to-layer separation is 250 μm. For the incident field propagating in "direction 1", the first- and second- order Bragg transmission dips are expected near 0.25 THz and 0.5 THz, since in that case the layer-to-layer separation is 400 μm. In this case, the second-order Bragg resonance is clearly identified, however the first-order resonance is too close to the magnetic resonance to be experimentally resolved.

A comparison of experiment with the finite-element simulation of the six-layer geometry shows satisfactory agreement [Fig. 7(a)(top)]. Additionally, a numerical comparison of closed-cylinder and open-cylinder transmittance in this range once again allows to identify the strong contribution of the magnetic resonance to the spectra, as well as allowing to isolate and

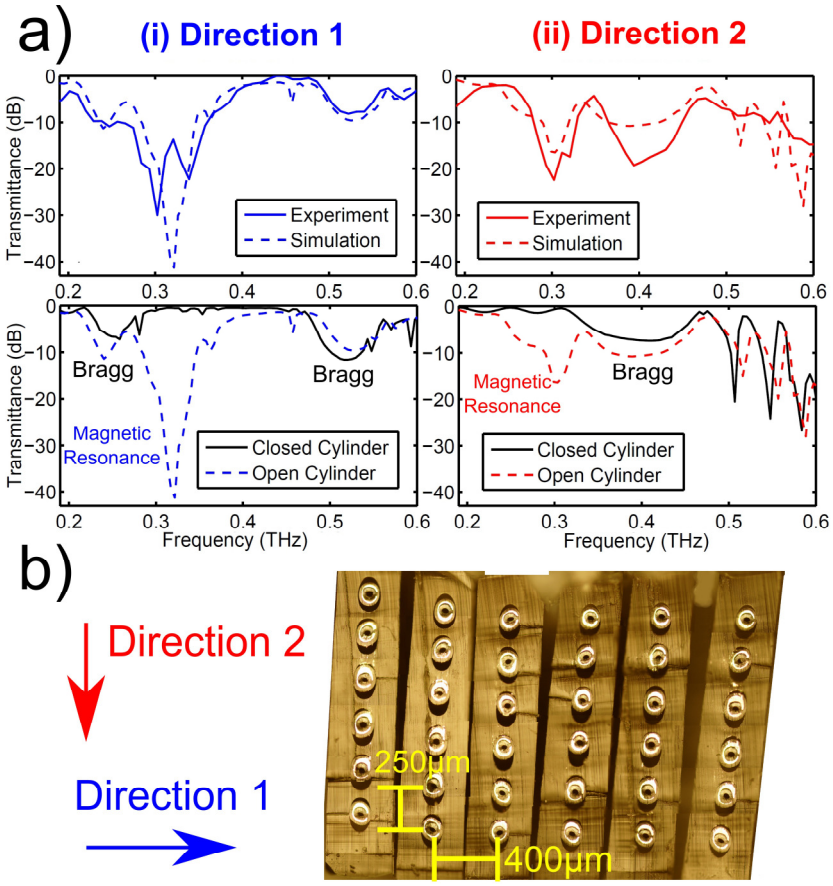

Fig. 7. (a) Top: experimentally measured and simulated transmittance for 6 sample layers with illumination under (i) direction 1 and (ii) direction 2. Bottom: numerically calculated transmittance of the six-layer metamaterial in each direction for open and closed cylinders. (b) Optical microscope image of the stacked 6-layer metamaterial, which was illuminated with a field propagating in direction 1 and direction 2.

identify the Bragg resonances mentioned [Fig. 7(b) (bottom)], which do not overlap significantly with the magnetic resonances for direction 1. Note however the discrepancy between experiment and simulation in Fig. 7(a)(i)(top), which is most pronounced near

#150223 - $15.00 USD Received 30 Jun 2011; revised 22 Jul 2011; accepted 22 Jul 2011; published 11 Aug 2011

resonance at 0.32THz, where the experiment shows a significantly higher transmission than simulation. Such behavior would in fact be expected if the Bragg resonance and magnetic resonance overlapped [41] as a consequence of the Fano-like interaction presented earlier [42]. However, experimental data suggests that this should not be the case, since a second-order Bragg resonance occurs at 0.52 THz, implying a first-order Bragg resonance at 0.26 THz. Other details of the experimental sample, for example the small differences in layer alignment and spacing, might explain this difference, since for simplicity our simulation considers only the ideal case (i.e. no spacing between layers and perfect alignment). Future work will aim at perfecting the multi-layer assembly technique and studying the interplay between Fano and magnetic resonances for such composite layer structures.

4. Conclusions

In conclusion, we have presented a novel procedure for fabricating scalable metamaterials with magnetic resonances from 0.1 to 0.4 THz via direct-fiber drawing. This technique potentially allows production of continuous metamaterials in very large quantities, literally by the kilometer. The time scales and skills involved in producing such lengths of metamaterial are similar to that of other microstructured polymer optical fibers; assembling the preform and drawing to fiber is quite straightforward and only requires a few hours. We have shown that such structures can be assembled into bulk three-dimensional metamaterials, for example multi-layers stacks. We have measured the transmittance with differing numbers of layers and under different illumination directions, finding good agreement with numerical simulations. We believe that under certain conditions Fano-like effects induce an increase in transmittance from the interference between Bragg and magnetic resonances. Such structures can for example form the building blocks of one-dimensional metamaterial photonic crystals exhibiting slow-light [42]. Additionally, stacking and drawing more complex preforms would result in sub-wavelength waveguides [43] or fibers with metamaterial claddings [44].

The procedure outlined in this paper can be scaled to smaller dimensions for operation at higher frequencies, by further drawing the structures presented here. Additionally, one should be able to extend this technique to direct-draw double-slotted-cylinder-resonators or swiss-roll geometries, to reduce the ratio of resonator size with respect to resonance wavelength. Combined with the previously presented fabrication of fiber-drawn metal-wire metamaterials [13] this could enable the development of woven negative index materials, as well as the fabrication of magnetic surface plasmon waveguides and subwavelength waveguides. Advanced weaving techniques could even allow production of materials with gradients of both positive and negative effective electric permittivity and magnetic permeability.

Acknowledgements

This work was performed in part at the Optofab node of the Australian National Fabrication Facility (ANFF) using Commonwealth and NSW State Government funding. ANFF was established under the National Collaborative Research Infrastructure Strategy to provide nano and microfabrication facilities for Australia's researchers. This material is based on research sponsored by the Air Force Research Laboratory, under Agreement No. FA2386-11-1-4049. The U.S. Government is authorized to reproduce and distribute reprints for Governmental purposes notwithstanding any copyright notation thereon. The views and conclusions contained herein are those of the authors and should not be interpreted as necessarily representing the official policies or endorsements, either expressed or implied, of the Air Force Research Laboratory or the U.S. Government. The work at the University of Wollongong was supported by the Australian Research Council. B.T.K. and A.A. acknowledge support from an Australian Research Council Future Fellowship and an Australian Research Fellowship, respectively.

#150223 - $15.00 USD Received 30 Jun 2011; revised 22 Jul 2011; accepted 22 Jul 2011; published 11 Aug 2011